SIMULATIONS OF THE SMOKE PARTICLE IMPACT DETECTOR(SPID) AND OBSERVATIONS DURING THE G-CHASER ROCKET CAMPAIGN

Henriette Trollvik[1], Tinna Gunnarsdottir[1], Ingrid Mann[1], Sveinung Olsen[1], Erlend Restad[2], Tarjei Antonsen[1], Åshild Fredriksen[1], Yngve Eilertsen[1], Ove Havnes[1], Rikke Hansen[1], Markus Floer[1], Arne Bjørk[2], Christopher Bootby[2], and Ralph Latteck[3]

[1]*Department of Physics and Technology, UiT The Arctic Univesity of Norway, 9019 Tromsø, Norway. Email: henriette.m.trollvik@uit.no*
[2]*Faculty of Engineering Science and Technology, UiT The Arctic Univesity of Norway, Narvik, Norway*
[3]*Institute of Atmospheric Physics, Kühlungsborn, Germany*

ABSTRACT

SPID, Smoke Particle Impact Detector, is a Faraday cup detector designed to measure nanometer-sized meteoric smoke particles during rocket flights. We report measurements made with SPID during the G-Chaser student rocket campaign 13 January 2019 and describe the design of the SPID instruments. Model calculations of dust trajectories within the detector result in an effective cross-section of 0.97 for particles larger than 0.5 nm at 60 km. Data analysis indicates that in order to generate the measured current, the number densities must be $\sim 10^{10}\mathrm{m}^{-3}$ or higher at 60 km. During the campaign the ground systems MAARSY and EISCAT were operating. These ground measurements showed smooth ionospheric conditions with weak precipitation down to 90 km. As a secondary goal of the campaign we wanted to investigate the possible connection between PMWE and MSPs. On the day of the launch there was no sign of PMWE and no conclusions can be drawn at this point.

Key words: Mesosphere; Dust; Sounding rocket; Grand Challange; G-Chaser; MSP; PMWE; DSMC; FEM.

1. INTRODUCTION

Since the mid 1900s the remnants of meteor ablation in the atmosphere have been studied (e.g [21], [14]). The residue of meteoric ablation in the atmosphere form the Meteoric Smoke Particles (MSPs). MSPs are believed to be important in the mesospheric charge balance, atmospheric chemistry [4], and phenomena such as Noctilucent Clouds (NLC), Polar Mesospheric Summer Echoes (PMSE) [19],[20], and possibly Polar Mesospheric Winter Echoes (PMWE) [16]. Over the years there have been several campaigns aimed at investigating MSPs, using rockets, combined with remote measurements such as radar and lidar observations, in addition to satellite observations (e.g [13], [20], [10], [2]). A majority of the research has been focused on the polar summer mesosphere, where the circulation pattern causes the temperature in the mesopause to drop bellow the local dew point of water. MSPs are believed to act as nuclei for the condensation of ice particles in the mesosphere ([20], [2]). The mesospheric temperature is higher in winter, ice particles can not exist and the smaller MSPs prevail. Models predict that the MSPs should have sizes ranging from 0.5-10 nm, dependent on their location in the atmosphere [e.g. [14], [19]]. The G-Chaser student rocket was launched from Andøya on the 13th of January 2019 09:13 UTC. Onboard was the Smoke Particle Impact Detector (SPID). SPID is designed to detect nanometer-sized meteoric smoke particles (MSPs) in the winter mesosphere.This article discusses the ionospheric conditions during the G-Chaser launch, it describes our simulations of the entry of small particles into SPID and presents the SPID measurements. It is structured in the following way: Section 2 contains details on the detector, section 3 contains information on the simulations and results. Section 4 gives an overview of the launch conditions. In section 5 we present the measurements made by SPID and some results and some conclusions are drawn in section 6.

2. SMOKE PARTICLE IMPACT DETECTOR SPID

SPID was designed to detect smoke particles in polar winter mesospheric conditions. It is based on heritage from previous Faraday cup dust detectors; such as the DUSTY and Multiple Dust Detector (MUDD) probes ([10], [2]). SPID is 251 mm high, including the electronic box under the detector, with a radius of 30 mm. It is designed with four grids and a solid middle plate consisting of seven concentric inclined rings. The grids are thin 0.25 mm silver wires. The vertical cross-section of the probe can be seen in Fig. 1. The grids are labeled GT1, GT2, MP, GB2, GB1, and the corresponding bias voltages are indicated. There are 50 mm high openings in the bottom

of the detector, to allow airflow through the instrument, transporting nanometer-sized particles through. SPID extends further out than the other payload parts. This is to bring it close to the shock front of the rocket to minimize deflection of small particles.

The top grid GT1 has a bias voltage of +10V to attract electrons and shield ions. The second grid is set to - 10V, to induce an electric field in between the grids and help transport the charged particles through. The middle plate has a bias of -2 V, chosen to help guide electrons and negatively charged particles away from the plate. The second to bottom grid GB2 has a potential of + 10 V, again to help guide the negative charge away from the middle plate. The last grid has a potential of -10V, inducing an electric field attracting ions and deflecting electrons. Currents are generated on the grids and on the middle plate by the triboelectric effect when interacting with the grids, this is discussed elsewhere in this issue [7].

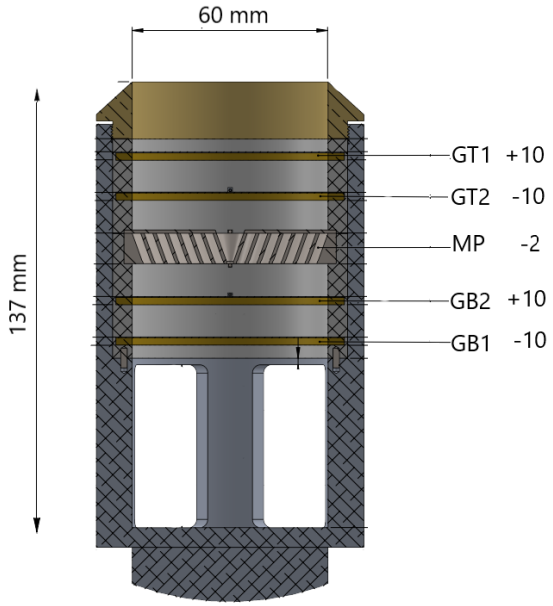

Figure 1. Vertical cross-section of the SPID probe, showing the grid design and interior. The grids and middle plate are indicated with their bias voltage.

Eq. 1 below states one way in which the current is related to the number density of dust particles, based on the work of Sagalyn et al [22], Havnes et al. [10] and personal communication with Havnes.

$$I = Av_r N_D e Z \sigma_{eff} \quad (1)$$

The particle amount is estimated using the volume a rocket traverses multiplied with the number density of the particles. The volume can be estimated by $V = Av_r$ where $A = \pi r_p^2$ is the area of the probe opening, r_p is the probe radius, v_r is the rocket velocity, e is the unit charge and Z is the charge number. Here we assume singly charged particles, the majority being positive and Z = +1. This is valid both for ions and MSPs. Not all particles will reach the middle plate, and furthermore, not all will hit the middle plate. To account for the loss of particles, the current is multiplied with an effective cross-section σ_{eff}. It is defined as the ratio of detection cross-section over the geometric cross-section. The estimation of σ_{eff} for SPID has been made using a dust and charge model from [4] based on work by [17], combined with the particle trajectory simulations. For a more detailed description see [25].

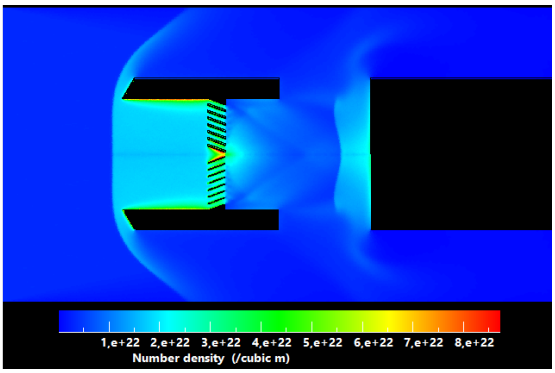

Figure 2. Result of the DSMC for January conditions for an altitude of 60 km. The linear color scale gives number density, with dark blue being the lowest and red the highest concentration.

3. SIMULATIONS

SPID traversed the atmosphere on the top deck of a sounding rocket. The rocket motion results in complex fluid dynamical effects, as the rocket will move from sub to supersonic speeds. Simulations were carried out on the dust flux into the instrument, both under the influence of the neutral gas and the influence of the electic field. The simulations are based on the methods described by [12] and [1].

3.1. Direct Simulation Monte Carlo

To simulate the neutral gas flow of the background winter atmosphere we have utilized the DS2V program developed by Bird, applying a Direct Simulation Monte Carlo (DSMC) method [5]. The input parameters are obtained from the MSIS-E-90 Atmosphere Model [6]. The simulation results shown in Fig. 2 are for a background atmosphere at 60 km with a background temperature of 247 K and number density of 3.47×10^{21} m^{-3}. The flow velocity was set to the rocket velocity which was 1595 ms^{-1} at 60 km. Fig. 2 shows that the number density inside the probe increases by a factor of 3, compared to the outside.

The airflow moves through, and after the middle plate, there are turbulent structures, as a result of the inclined design of the plate. In addition to facilitating the flow through the detector, the open design reduces the size of the shock front, and thus reduces the amount of deflected particles. For a blunt body the shock front is proportional to the probe radius, and in the case for SPID it has been reduced to several times less [23].

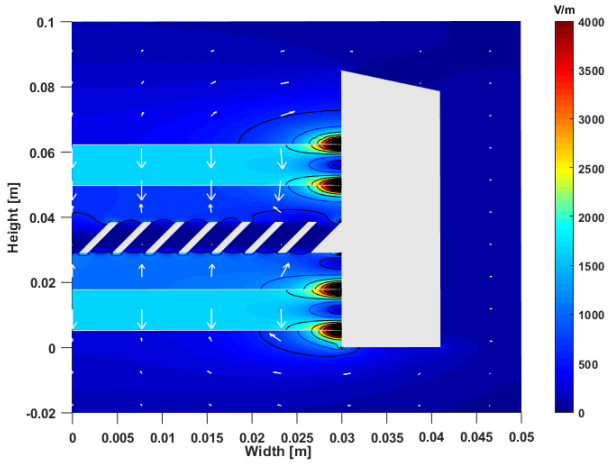

Figure 3. FEM results of the electric field inside SPID. The color scale has been adjusted to enhance the strong and weak sections of the probe. The arrows indicate the direction of the electric field, and the size of the arrows the relative strength.

3.2. Finite Element Method

The electrically biased grids in SPID induce an electric field. In order to investigate the effect of the electric field on the charged particles, we simulated the 2D electric field structure using a finite element method (FEM). The rotational symmetry of the probe allows for symmetric solutions. The finite element method divides the geometry into small parts and solves the Laplace equation. The solution of the FEM is shown in Fig. 3, where blue indicates weak, and red indicates strong $|E|$ field. Note that the color scale has been adjusted to enhance the differences. The edge effects generate strong fields, and the simulations suggest an E field with strength reaching $10^4 \mathrm{Vm}^{-1}$. This occurs in the corners where the grids are connected to the probe walls, and at the edges of the middle plate. Whether these edge effects are applicable to a real physical instrument is still unclear. The potential structures result in close to homogeneous E field along the center axis of the probe.

3.3. Particle trajectory

The dust particles are effected by three forces; the gravitational force, the drag force from the neutral gas and the charged particles are additionally effected by the Coulomb force. The full expression for the dust dynamics can be found in the appendix, where Eq. 2 states the resulting equation of motion for individual smoke particles. The drag force is derived based on the assumption that the dust particle mass is much larger than the neutral gas mass, and assuming particles of spherical shape.

Pre-flight we did simulations with an assumed rocket velocity of 1000 ms^{-1}. It showed that particles down to a size limit around 0.8 nm radius could enter the detector. It turned out that the rocket traversed the mesosphere with an average velocity of 1400 ms^{-1}, and at 60 km it had a velocity of 1600 ms^{-1}. New simulations, accounting for the high velocity were made, suggesting that particles down to 0.4 nm could enter the detector. This is on the limit of the model application, since the dust mass approaches the background gas limit. Fig. 4 shows the trajectories for negatively, neutrally and positively charged particles, from left to right respectively. The simulations are for particles with a radius of 0.8 nm at 60 km. The trajectories are very similar, but close to the edges the trajectories vary as a result of the induced electric field. The neutral particles follow the neutral flow, as they will not be affected by the induced field. Right before the entrance of the probe the particle trajectories have a small horizontal shift in the trajectory, as a result of the shock front. The negative particles are deflected from the edges, and the positive particles are attracted. These edge effects are the result of the electric field structure that can be seen in Fig. 3.

The simulations were carried out for a range of sizes (0.5 to 8.6 nm), and by assuming a size and charge distribution based on the work by [17] and [4]. The simulation results were combined to find an effective cross-section. At 60 km, only counting the particles hitting the middle plate directly, the cross-section of SPID is estimated to 0.3. However, including all the particles that pass the middle plate the estimated cross-section increases significantly to 0.97. This suggests that a substantial amount of particles will enter the probe, assuming the radii of particles are between 0.5 and 8.6 nm. Due to the uncertainties in the detection procedure it is likely that the particles do not have to hit the plate directly to generate charge. As a result we expect the effective cross-section to lie closer to 0.97 than 0.3.

4. LAUNCH CONDITIONS

The G-Chaser rocket was launched from Andya Space Center (69°N and 16°E) at 09:13 UTC on the 13th of January 2019. As part of the mission we wanted to investigate the possible relation between PMWE and MSPs. The ground systems MAARSY and EISCAT were running during the campaign. The PMWE activity is at its lowest in January, with an occurrence rate of 10% [16]. The multibeam radar system MAARSY, operates at 53.5 MHz [15]. The days prior to the launch of G-Chaser showed PMWE activity, however there were no PMWE

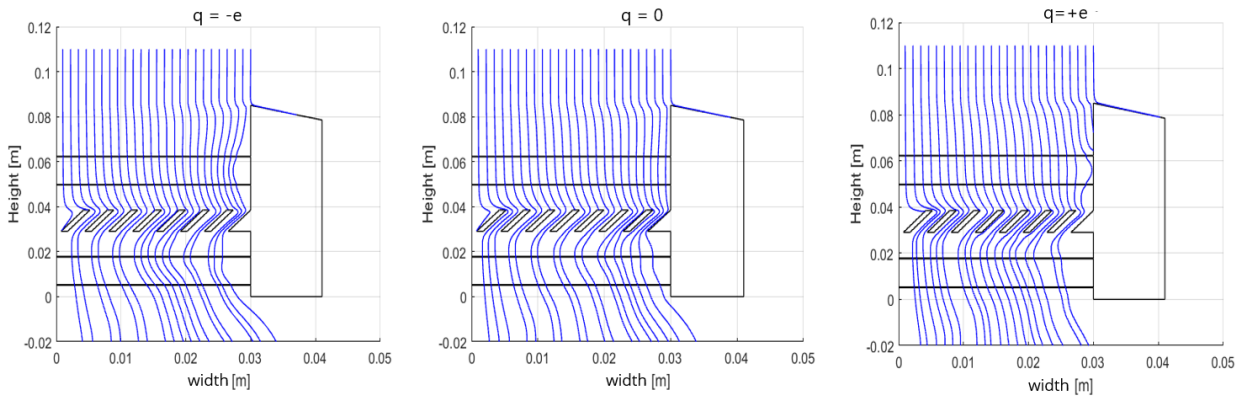

Figure 4. Particle trajectories from left to right are the trajectories for negative, neutral and positively charged particles respectively. The simulations are done for MSPs with a 0.8 nm particle radius with background conditions corresponding to 60 km.

activity at time of the launch. The two EISCAT radar systems at Ramfjordmoen (69°N and 19°E) were operated during the campaign. The VHF (224 MHz) was running the manda program suitable for D region observation with high resolution, pointing in the vertical direction. The UHF (933 MHz) was running the arc1 program suitable for investigations of the E/F region with very high temporal resolution, and it was pointed in the predicted rocket trajectory. The EISCAT observation show weak electron precipitation down to $\sim$ 90 km, but otherwise calm atmospheric conditions. The electron density was too low for EISCAT to derive ionospheric parameters below 80 km. The ground magnetometers close to Andøya did not show strong magnetic variations [9].

5. MEASUREMENTS AND RESULTS

In this section we present some of the measurements and results from SPID. The three bottom grids of SPID measured a strong current starting right after the nosecone was separated and for the remaining part of the rocket trajectory. The two top grids became saturated after the nosecone was separated, those signals were not used for the data analysis. The entire flight was $\sim$ 4 min, and the rocket hit a dense atmosphere at $\sim$ 20 km on the down leg. The raw currents (nA) from the three bottom grids, MP, GB2, GB1, from top to bottom) are plotted in Fig. 5. The currents are shown as a function of time, from the nosecone separation at 53 km and until 110 sek, corresponding to $\sim$ 129 km. It should be noted that the current scales are different in each figure.

On the payload there were instruments that required a smaller spin, and the rocket had to despin. This reduced the spin from 5 Hz to 1 Hz, which can be seen in the two bottom plots at 67 sec. The lower spin also resulted in a larger precession on the rocket, which is also visible in the signal. In this paper we have focused on the middle plate signal. Around 55 sec there is a clear peak in the signal.

Fig. 6 on the left shows a detailed view of the lower altitude middle plate signal. There is a strong increase in the signal right after the nosecone is separated. The current has a maximum value of 17nA. Fig. 6 on the right shows the corresponding power spectrum of the signal. The power spectrum was found using a wavelet analysis. The spectrum is shown as a function of altitude and wavelength. There are three clear spikes in the signal, one at 56 km, one at 57 km and one wide at 61.5 km. In addition there is some high frequency noise visible at the far right of the spectrum which has not been investigated further at this point. From the current we can deduce an estimated density by combining the simulation results with the measured current. Eq. 1 in section 3 is applied to the measured current, in addition to estimated values for the remaining terms. The densities required to explain a current of $I = 17$nA, depending on the different values of σ_{eff}, varies from $2 * 10^{10}$ to $2 * 10^{11}$ m^{-3}. This is for a rocket velocity of $v_r = 1600$ ms^{-1}, same as the velocity of SPID at $\sim$ 57 km, and a probe radius of $r_p = 0.03$m. As the density is inversely dependent on σ_{eff} the number density increases by a factor of 10 for the small values, compared to that for large values. With an effective cross-section of 0.8, the number density should be around $2 * 10^{10}$ m^{-3}. This is close to the reported values on both the ion and MSP density. Hence at this point more investigations are needed to explain the source of the measured current.

The current fluctuations present are low frequency, with wavelengths on the order of 10^2 to 10^3 m. The strongest spike in the wavelet analysis is at 57 km, but only reaches $\sim$ 10 m, still way below the bragg scale of MAARSY and EISCAT.

6. CONCLUSION

In this paper we have presented some of the preliminary results from SPID measurements during the G-Chaser campaign. The particle trajectory simulations made for

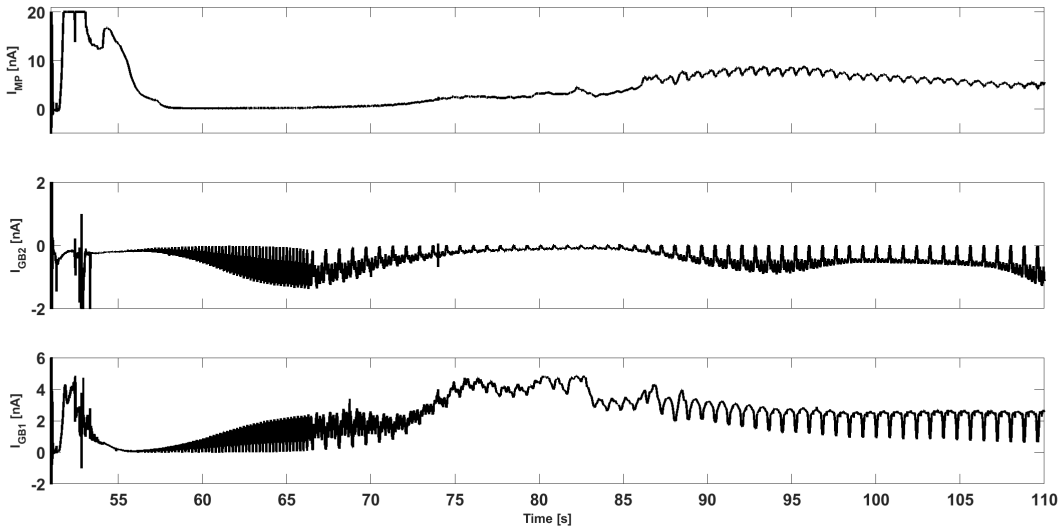

Figure 5. Raw current from when the nosecone is separated and to 110 sek where the rocket is approaching 130 km. The current is in units of nA. The figures on top to bottom is MP, GB2 and GB1 respectively. All three grids show strong variations in the current in the lower altitudes, MP with the strongest signal reaching $\sim$ 17 nA, not including the saturated regions.

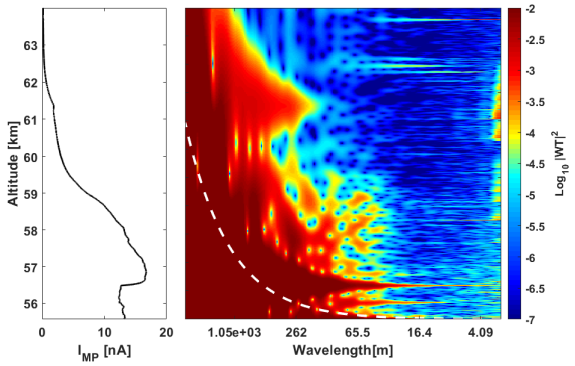

Figure 6. Comparison of the raw current and the power spectra, estimated using a wavelet transform, for altitudes between 53 to 65 km . The left panel shows the raw middle plate current in nA. Above 63 km, the signal decreases until it is $\sim$ 0. The figure on the right shows the power spectrum of the amplitude at the same altitude as given on the left, as a function of wavelength.

the instrument suggest an effective cross-section of 0.97. This suggests that a substantial amount of particles entered the probe, including small particles. The ground observations show no sign of PMWE, and low electron density. The measurements from SPID suggest a layer of particles with number density of 10^{10} m^{-3} or higher to explain a current of 17nA. Whether this larger current around 60 km is generated by ions, MPSs or both cannot be concluded at this point, but it is reasonable to assume that it might be a combination. Further work will focus on determining the background current. Thorough simulation on the ion motion should be conducted, and combined with ion concentration models.

ACKNOWLEDGEMENTS

The work of the UiT team was supported by The Norwegian Research Council under the projects NFR 275503 and 240065. The UiT Rector's funds, UiT Department of Physics and Technology and UiT Faculty of Engineering and Technology. The Norwegian Space Agency contributed funded student travels to the integration at NASA Wallops Flight Facility and the launch at Andøya Space Center.

The SPID team consisted of two groups. The Narvik group was in charge of the electronics part. It included Arne Bjørk, the coordinator for the Narvik students; Erlend Restad, Christofer Boothby, James Alexander Cowie, Vetle Tronstad and Christer Nordby. The Tromsø group was in charge of the design and development of the instrument, participated in some of the electrical work, and handled the data processing and analysis. The group consisted of Åshild Fredriksen who was the coordinator for UiT group; Ove Havnes, Tarjei Antonsen, Ingrid Mann, Sveinung Olsen, Ynvge Eilertsen, Tinna Gunnarsdottir, Henriette Trollvik, Rikke Hedelund Hansen and Markus Floer.

The Middle Atmosphere Alomar Radar System (MAARSY) is operated on Andya by the Leibniz-Institute of Atmospheric Physics e.V. at the University Rostock, Kühlungsborn, Germany. The EISCAT VHF and UHF radars are operated at Ramfjordmoen near

Table 1. Constants in particle trajectory simulation. Figure adapted from Antonsen et al. [1]. The numbers stated are for MSPs.

Symb.	Description	Value
ρ_d	MSP mass density	3000 kgm^{-3}
m_D	Mean dust weight	140 amu
L	Latent heat vaporization	$6 \cdot 10^6$ Jkg^{-1}
c_p	Specific heat	1000 Jkg^{-1}K^{-1}
$\bar{\gamma}_{MSP}$	Mean surface energy	0.200 Jm^{-2}

Tromsø by EISCAT. EISCAT is an International Association supported by the Research Councils of Finland (SA), France (CNRS), the Federal Republic of Germany (MPG), Japan (NIPR), Norway (NFR), Sweden(VR), and the United Kingdom (PPARC).

APPENDIX A

The equation of motion of the dust particles in the high velocity regime includes a complex drag force due to the background gas. Eq. It is derived by [1] based on work by [3] and [24]. The drag term is dervived with the assumption that the mass of the dust particle is much larger than the mass of a background gas molecule. In addition it is assumed that the particles are spherical. Fig. 2 states the equation of motion used

$$\begin{aligned} m_d \frac{d\vec{v}_d}{dt} =& m_d\vec{g} + q_d\vec{E} + \pi r_d^2 m_g n_g v_{th,g}(\vec{v}_g - \vec{v}_d)\frac{1}{u} \\ & * \left\{ \frac{1}{\sqrt{\pi}} \left(u + \frac{1}{2u} \right) \exp(-u^2) \right. \\ & \left. + \left(1 + u^2 - \frac{1}{4u^2} \right) \text{erf}(u) \right\} \end{aligned} \tag{2}$$

where m_d is the mass of a dust grain. $\vec{v}_d$ denotes the vector velocity of the dust particle. We have considered a 2D case, where the dust can only move sideways or downwards, inferring the rotational symmetry of the probe. The right side of the equation the three forces are considered. First is the gravitational force, with the acceleration due to gravity as g, in the case for 60 km at northern latitudes is ~ 9.66 ms^{-2}. This only has a component in the vertical direction, assuming down in the instrument is radially downwards to earth. The second component is the Coulomb force, where q is a unit charge and E is the electric field. The electric field solution is exported from the FEM simulations. The last term is the drag force on the dust particle due to the neutral flow. Tab. 1 lists the symbols and their meaning in addition to the values we used. Most of the values are dependent on the composition, and for our case the values listed are for MSPs. $u = \frac{|\vec{v}_d - \vec{v}_g|}{v_{th,g}}$ is the normalized relative atom flow speed and $v_{th,g} = \sqrt{\frac{2k_B T_g}{m_g}}$ is the thermal velocity. Eq. 2 is an ordinary differential equation and solved by the Runge Kutta method.

REFERENCES

[1] Antonsen, T. (2013). On the internal physical conditions in dust probes: transport, heating and evaporation of fragmented dust particles (Master's thesis, UiT Norges arktiske universitet).

[2] Antonsen, T., Havnes, O., & Mann, I. (2017). Estimates of the Size Distribution of Meteoric Smoke Particles From RocketBorne Impact Probes. Journal of Geohttp://prettymuchamazing.com/physical Research: Atmospheres, 122(22), 12-353.

[3] Baines, M. J., Williams, I. P., Asebiomo, A. S., & Agacy, R. L. (1965). Resistance to the motion of a small sphere moving through a gas. Monthly Notices of the Royal Astronomical Society, 130(1), 63-74.

[4] Baumann, C., Rapp, M., Anttila, M., Kero, A., & Verronen, P. T. (2015). Effects of meteoric smoke particles on the D region ion chemistry. Journal of Geophysical Research: Space Physics, 120(12), 10-823.

[5] Bird, G. A. (2005, May). The DS2V/3V program suite for DSMC calculations. In AIP conference proceedings (Vol. 762, No. 1, pp. 541-546). AIP.

[6] Chulaki, A (n.d). MSIS-E-90 Atmosphere Model. Retrieved from https://ccmc.gsfc.nasa.gov/modelweb/models/msis_vitmo.php

[7] Gunnarsdottir, T., Trollvik, H., Mann, I., Olsen, S., Eilertsen, Y., Antonsen, T., Havnes, O., Bjørk, A., Restad, E., Fredriksen, ., Boothby, C., Hansen, R.H., & Floer, M. (2019). Charging and detection of mesospheric dust with instruments SPID on G-Chaser rocket. In this publication.

[8] Gunnarsdottir, T. (2019). Charging Effects and Detection of Mesospheric Dust with the Instrument SPID on the G-Chaser Rocket (Master's thesis, UiT Norges arktiske universitet).

[9] Hall, C. (2019). Magnetometer Stackplot Troms Geophysical Observatory. Retrieved from http://flux.phys.uit.no/stackplot/

[10] Havnes, O., Trim, J., Blix, T., Mortensen, W., Nsheim, L. I., Thrane, E., & Tnnesen, T. (1996). First detection of charged dust particles in the Earth's mesosphere. Journal of Geophysical Research: Space Physics, 101(A5), 10839-10847.

[11] Havnes, O., Latteck, R., Hartquist, T. W., & Antonsen, T. (2018). First simultaneous rocket and radar detections of rare low summer mesospheric clouds. Geophysical Research Letters, 45(11), 5727-5734.

[12] Hedin, J., Gumbel, J., & Rapp, M. (2007). On the efficiency of rocket-borne particle detection in the mesosphere. Atmospheric Chemistry and Physics, 7(14), 3701-3711.

[13] Hervig, M. E., Deaver, L. E., Bardeen, C. G., Russell III, J. M., Bailey, S. M., & Gordley, L. L. (2012). The content and composition of meteoric smoke in mesospheric ice particles from SOFIE observations. Journal of Atmospheric and Solar-Terrestrial Physics, 84, 1-6.

[14] Hunten, D. M., Turco, R. P., & Toon, O. B. (1980). Smoke and dust particles of meteoric origin in the mesosphere and stratosphere. Journal of the Atmospheric Sciences, 37(6), 1342-1357.

[15] Latteck, R., Singer, W., Rapp, M., Vandepeer, B., Renkwitz, T., Zecha, M., & Stober, G. (2012). MAARSY: The new MST radar on Andøya - System description and first results. Radio Science, 47(01), 1-18.

[16] Latteck, R., & Strelnikova, I. (2015). Extended observations of polar mesosphere winter echoes over Andøya (69 N) using MAARSY. Journal of Geophysical Research: Atmospheres, 120(16), 8216-8226.

[17] Megner, L., Siskind, D. E., Rapp, M., & Gumbel, J. (2008). Global and temporal distribution of meteoric smoke: A twodimensional simulation study. Journal of Geophysical Research: Atmospheres, 113(D3).

[18] Plane, J. M. C., Cox, R. M., & Rollason, R. J. (1999). Metallic layers in the mesopause and lower thermosphere region. Advances in Space Research, 24(11), 1559-1570.

[19] Plane, J. M., Feng, W., & Dawkins, E. C. (2015). The mesosphere and metals: Chemistry and changes. Chemical reviews, 115(10), 4497-4541.

[20] Rapp, M., Strelnikova, I., Strelnikov, B., Latteck, R., Baumgarten, G., Li, Q., ... & Robertson, S. (2009). First in situ measurement of the vertical distribution of ice volume in a mesospheric ice cloud during the ECOMA/MASS rocket-campaign. Annales Geophysicae, 27, 755766.

[21] Rosinski, J., & Snow, R. H. (1961). Secondary particulate matter from meteor vapors. Journal of Meteorology, 18(6), 736-745.

[22] Sagalyn, R. C., Smiddy, M., & Wisnia, J. (1963). Measurement and interpretation of ion density distributions in the daytime F region. Journal of Geophysical Research, 68(1), 199-211.

[23] Shankara, T. S., & Sreekanth, A. K. (1977). Shock standoff distance for a sphere. Journal of Applied Physics, 48(4), 1765-1765.

[24] Smirnov, R. D., Pigarov, A. Y., Rosenberg, M., Krasheninnikov, S. I., & Mendis, D. A. (2007). Modelling of dynamics and transport of carbon dust particles in tokamaks. Plasma Physics and Controlled Fusion, 49(4), 347.

[25] Trollvik, H. M. T. (2019). On the Meteoric Smoke Particle Detector SPID: Measurements and analysis from the G-chaser rocket campaign (Master's thesis, UiT Norges arktiske universitet).